Research Article

Nano Biomed Eng

Kickxia elatine-assisted Bio-fabrication of Nano-silver and Their Antioxidant, Anti-alpha Amylase, and Anti-acetylcholinesterase Properties

Noor Ul Huda[1], Mushtaq Ahmed[1], Nadia Mushtaq[2], Rahmat Ali Khan[1]

[1] Department of Biotechnology, University of Science and Technology Bannu, Bannu, Pakistan
[2] Department of Botany, University of Science and Technology Bannu, Bannu, Pakistan

Corresponding author. E-mail: mushtaq213@yahoo.com

Received: Feb. 4, 2023; **Revised:** May 3, 2023; **Accepted:** May 12, 2023

Citation: N.U. Huda, M. Ahmed, N. Mushtaq, et al. *Kickxia elatine*-assisted bio-fabrication of nano-silver and their antioxidant, anti-alpha amylase, and anti-acetylcholinesterase properties. *Nano Biomedicine and Engineering*, 2023, 15(2): 150−169.

http://doi.org/10.26599/NBE.2023.9290021

Abstract

Green synthesis of silver nanoparticles (AgNPs) is attaining more attention from researchers over chemical fabrication due to their unique properties such as high dispersion in solution, surface-to-volume ratio, low toxicity, and easy preparation. In this paper, a biogenic synthesis of *Kickxia elatine*-based-silver nanoparticles (KE-AgNPs) was carried out by using *K. elatine* plant extract (KEE). The characterization of synthesized AgNPs was done by ultraviolet (UV) spectroscopy, scanning electron microscopy (SEM), X-ray diffraction (XRD), energy-dispersive X-ray (EDX), and Fourier transform infrared (FTIR) analyses. XRD screening confirmed the crystalline nature of KE-AgNPs with 42.47 nm in size. SEM analysis confirmed the rounded shape AgNPs with 50 nm in size. FTIR confirmed the various functional groups that contribute to the stabilization and reduction of AgNPs. EDX displayed an intense peak (3.2 keV), presenting that Ag has a chief component with 61.67%. These AgNPs showed a potential antioxidant activity against 2,2'-azino-bis-(3-ethyl) benzothiazoline-6-sulfonic acid (ABTS, 66.9%), diphenyl-1-picrylhydrazyl (DPPH, 72.49%), H_2O_2 (69.42%), ferric-reducing antioxidant power assay (FRAP, 70.04%), and ammonium molybdenum (68.77%) at the highest concentration of 160 μg/mL. Statistical analysis showed that both KEE and their AgNPs inhibit alpha-amylase (α-amylase) in the mixed type mode, i.e., Michaelis constant (K_m) increased (16.62%–55.45% and 49.77%–134.78% for KE-AgNPs) and V_{max} decreased (2.68%–12.98% and 4.44%–11%), respectively. In the case of anti-acetylcholinesterase studies, both KEE and AgNPs revealed a mixed-type inhibition against acetylcholinesterase (AchE), i.e., K_m increased (13.53%–101.48% and 10.10%–38.04%), while V_{max} decreased (12.66%–52.47% and 11.91%–41.69%) for KEE and KE-AgNPs, respectively. Therefore, the synthesized AgNPs could be used for various purposes due to their non-toxicity, eco-friendly, and compact ability for therapeutic and diagnostic applications.

Keywords: *Kickxia elatine*; silver nanoparticles (AgNPs); antioxidant activity; α-amylase; acetylcholinesterase; kinetics; nanotechnology

Introduction

Recently, nano science and technology are gaining enormous attention all over the world for solving different problems in the fields of pharmacology, biomedicine, and food processing and packing. The

nanoparticles (NPs) may be defined as atomic or molecular scale solid nanometer-sized particles ranging from 1 to 100 nm in size and having unique optical, physical, and chemical properties [1, 2]. These NPs are usually synthesized using metals such as gold, zinc, copper, iron, silver, and platinum [3]. Among NPs, silver nanoparticles (AgNPs) have versatile applications in the field of medicine and biology because of outstanding properties such as high dispersion in solution and surface-to-volume ratio [4]. AgNPs are extensively used as antimicrobial, antioxidant [5], acetylcholinesterase (AchE) inhibitors [6], and anti-diabetic agent [7]. Reactive oxygen species (ROS) are the substances that cause oxidative stress and have harmful effects on cell structure and function that lead to various diseases [8, 9]. NPs demonstrated a distinctive cellular interface with ROS and possessed considerable scavenging potential as compared with ascorbic acid [10]. The enzyme α-amylase is involved in the catabolism of starch and glycogen into glucose and maltose and elevates blood glucose levels. AgNPs reduce carbohydrate digestion by inhibiting α-amylase and can be used as hypoglycemic agent [11]. The physical and chemical methods of synthesis of AgNPs have limitations for being costly and inclusion of toxic solvents. Currently, researchers are using green methods for the biosynthesis of AgNPs where the bio-extracts are used as capping and reducing mediators for the fabrication of AgNPs. These mediators (saponin, alkaloids, flavonoids, phenols, tannin, etc.) act as reducing agents for Ag^+ to generate NPs [12]. Recently reported plant extracts that were used for biosynthesis of AgNPs included *Urtica diocia* [13], *Tropaeolum majus* [14], *Skimmia laureola* [15], *Azadirachta indica* [16], and *Araucaria angastifolia* [17].

Kickxia is a genus of the family Plantaginaceae, comprised of 47 species commonly known as cancerworts or fluellins [18]. *Kickxia elatine* (KE) is an annual plant used in conventional medicine as wound-healing agent, sedative, general tonic, and also in case of bleeding and lacrimation [19]. Worldwide only a few species of *kickxia* have been analyzed for its phytochemical constituents which result in the isolation of flavonoids and iridoid glycosides [20], which conferred gooantiglycationon activity (inhibition of α-glycosidase). Yuldashev extracted four types of flavonoid (flavone, glycosides, pectolinarin, and acetylpectolinarin) from *K. elatine* which suggests its strong antioxidant activity and prevents the development of heart ailment, cancer, diabetes, and some other disorders like Alzheimer's and dementia [21,22]. Other related species like *Kickxia ramosissimia* is used for the treatment of kidney stone [23], fever and rheumatism [24], snake and scorpion bites [25], cytotoxicity [26], and diabetes mellitus [21]. Linarioside extracted from *Kickxia spuria*, *K. elatine* (L.) *Dumort*, and *Kickxia commutata* expressed strong anti-diabetic activities [27].

K. elatine is one of the least explored members of Plantaginaceae. Its anti-diabetic, antioxidant, and acetylcholinesterase inhibitory activity has not been evaluated previously. The present work is based on the hypothesis that *K. elatine* plant extract (KEE) and synthesized KE-AgNPs will bear effective anti-diabetic, free radical scavenging, and anti-Alzheimer activity due to the presence of biologically active ingredients in KEE.

Materials and Methods

K. elatine collection and processing

The plant *K. elatine* was procured in June from KP, Pakistan (District Bannu). The plant was identified by a professional taxonomist Dr. Tahir Iqbal and a voucher specimen was recorded (NH II) at the University of Science and Technology (UST), Bannu. The whole plant was cleaned with distilled water, dried in shade, and ground to finest powder. About 300 g of KE milled powder was extracted in 1.5 L of ethanol, agitated for 5 h at 120 r/min on an orbital shaker and kept for 7 days. After a week, the extract was sieved with Whatman filter paper. Extra ethanol was evaporated with a rotary evaporator from the extract. The concentrated KEE was air-dried at 37 ℃ and achieved at 4 ℃.

Biosynthesis of KE-AgNPs

KE-AgNPs were generated using a standard procedure [28]. For the preparation of KE aqueous extract, accurately measured 1.5 g of KE crude extract was mixed with 100 mL of deionized water, and stirred for complete dissolution. Centrifugation of the solution was done at 6000 r/min for half an hour. The pellet was discarded and supernatant was kept for use in production of AgNPs. About 1 L of the 1 mmol/L $AgNO_3$ salt solution was prepared and the pH was set to 9. After that, the supernatant (KE aqueous extract) was dissolved in 1 mmol/L $AgNO_3$

solution in a 1:10 ratio. The resulting mixture color changing to reddish-brown after an hour was an indication of chemical reduction (formation of KE-AgNPs). For maximum reaction, the solution was further incubated at 40 ℃ for 24 h. Ultraviolet–visible (UV–Vis) spectrometry between 300 and 800 nm validated the production of AgNPs. KE-AgNPs were separated at −4 ℃ by cold centrifugation at 14 000 r/min. The obtained NPs pellet was dried in an incubator at 50 ℃ and used for further characterization.

Intrinsic factors affecting synthesis of AgNPs

To assess the factor affecting the formation of KE-AgNPs, different volumes (0.25–2 mL) of KEE were used. To assess the impact of temperature and time, AgNPs were produced at different temperatures of 20, 40, 60, 80, and 100 ℃ and varied time (1, 2, 3, and 24 h). To analyze the effect of Ag-salt concentration, four different dilutions (0.5, 1, 1.5, and 2 mmol/L) of Ag-salt were created. To assess the pH effect, the pH of 1 mmol/L $AgNO_3$ salt solution was maintained from 5 to 12, respectively. Further, KE-NPs stability was tested after 1, 30, and 90 days.

Characterization of KE-AgNPs

AgNPs formation was confirmed by UV–Vis spectrometry between 300 and 800 nm. Fourier transform infrared (FTIR, Nicolet iS50 FTIR) spectra of KEE and KE synthesized NPs were acquired to examine the phytochemicals and different functional groups in the infrared (IR) radiation range of 400−4 000 cm^{-1}. The KE-AgNPs crystalline structure was analyzed using the JEOLX-ray diffractometer (XRD) model JDX-3532 (Japan). The size and shape morphology of the biosynthesized KE-AgNPs was validated by scanning electron microscopy (SEM). Energy-dispersive X-ray (EDX) spectroscopy was done to examine the presence of silver and other elements in fabricated KE-AgNPs.

Antioxidant activities

Assessment of 2,2'-azino-bis-(3-ethyl) benzothiazoline-6-sulfonic acid (ABTS) radicals hunting assay

The ABTS radicals were produced by incubating a combination of 7 mmol/L ABTS with 2.45 mmol/L potassium per sulfate ($K_2S_2O_8$) for an entire night. Deionized water was used to dilute the mixture, resulting in an optical density of 0.85 (± 0.20). About 300 µL of different sub solutions of standard ascorbic acid (AA), KEE, and KE-AgNPs (100, 200, 300, and 400 µg/mL, stock solution 1 mg/mL) were supplemented to 3 mL of ($K_2S_2O_8$+ABTS) mixture, respectively, incubated for 4 min and at 734 nm, absorbance was calculated against water as blank. To eliminate the errors, the process was repeated 3 times [28]. ABTS scavenging strength was assessed as follows:

$$\text{Percent scavenging} = \frac{\text{absorbance of contral} - \text{absorbance of test sample}}{\text{absorbance of contral}} \times 100\% \quad (1)$$

Diphenyl-1-picrylhydrazyl (DPPH) activity

About 200 µL of the test sample was dissolved in 800 µL of DPPH (3 mg/100 mL methanol) and allowed to 30 min dark-incubation at room temperature. After this, at 517 nm, absorbance was measured. Ethanol was utilized as a blank. DPPH scavenging ability was measured by comparing the results of the test sample and control [29].

Hydrogen peroxide scavenging bioassay

A typical procedure was adopted to analyze the H_2O_2 activity [30]. In a test tube, 400 µL of 50 mmol/L phosphate buffer (pH = 7.4) and 400 µL of 2 mmol/L H_2O_2 were combined with 200 µL of sub-solutions of KEE, KE-AgNPs, and AA and, mixed well. At 610 nm, absorbance was documented against phosphate buffer as a reference. The H_2O_2 inhibition potential was measured by Eq. (1).

FRAP

The FRAP potential of KEE and KE-AgNPs was calculated by the standard method [31]. About 1 mL of the sample was treated with an equivalent volume of 1% potassium ferro cyanide and 0.2 mol/L phosphate buffer at pH = 6.6 and subjected to 20 min incubation at 50 ℃. Furthermore, 1 mL of trichloroacetic acid (100 mg/mL) was transferred to the solution to stop the reaction. About 2 mL of the above working mixture was combined with 2 mL of deionizing water and 0.4 mL of ferric chloride (0.1%) and incubated for 10 min. The absorbance of the mixture was measured at 700 nm.

Ammonium molybdenum antioxidant assay

For assessment of the ammonium molybdenum antioxidant capability of KE-AgNPs and KEE, the standard procedure was used [32]. About 300 µL of the KE-AgNPs and KEE was added to 3 mL of

ammonium molybdenum reagent (4 mmol/L ammonium molybdenum, 28 mmol/L sodium phosphate, and 600 mmol/L H_2SO_4) and allowed to incubation for 1.5 h at 95 ℃. Further, the mixture was cooled to room temperature and the absorbance was documented by double beam UV-1602, BMS-spectrophotometer at 695 nm.

In-vitro hypoglycemic (α-amylase) assay

The capability of KEE and its nanoparticles on α-amylase inhibition was evaluated by the following standard protocol [33]. To make a 1% starch solution, about 1 g of potato starch was supplemented to 100 mL of 16 mmol/L sodium acetate buffer (pH = 6.9) to create 1% starch solution. About 250 µL of different sub solutions (25, 50, 75, and 100 µg/mL) of KE, KE-AgNPs, and glucophage (control) was dissolved in 250 µL of α-amylase (1 mg/2 mL) and allowed for 10 min incubation. Further, 250 µL of the starch solution was dissolved in this mixture and incubated again for 10 min. About 250 µL of 3,5 dinitrosalicylic acid (DNSA) color reagent was dissolved in the above mixture to block the reaction and subjected to incubation for 5 min at 90 ℃, chilled to 25 ℃, and diluted with distilled water in 1:5. The reaction absorbance was recorded at 450 nm against deionized water. The percent inhibition was deliberated by Eq. (1).

Mode of inhibition of α-amylase

To analyze the type of inhibition against α-amylase, the same protocol was employed as designated earlier [33]. About 250 µL of α-amylase (1 mg/2 mL) and 250 µL of different sub-solutions (25, 50, 75, and 100 µg/mL) of the test inhibitors were pre-incubated. The reactions were initiated by the addition of 100, 200, and 300 mg (0.1%, 0.2%, and 0.3%) potato starch, followed by 10 min incubation at 25 ℃. To terminate the reaction, about 0.25 mL DNSA was added to the mixture. The solution was incubated for 5 min at 90–95 ℃, cooled, and diluted, and absorbance of mixture was assessed at 450 nm. The $1/V$ vs. $1/[S]$ (double reciprocal plot) plot was designed, where V represents velocity of the reaction and $[S]$ represents potato starch (substrate) concentration [34]. Michaelis–Menten kinetics was used to analyze the Lineweaver–Burk plot and determine the kind of inhibition. The K_m was calculated by two different plots of $1/V$ vs. $1/S$ and V vs. V/S [35]. Cornish–Bowden plots (S/V vs. I) were plotted to evaluate inhibition constant (K_i). Dissociation constant (K_I) was calculated by scheming the Dixon plot ($1/V$ vs. I) [36]. IC_{50} was computed by percent activity and percent inhibition versus concentration of KEE and KE-AgNPs.

Enzyme preparation (venom)

Venom was manually squeezed out from *Bungarus sindanus* snakes, then lyophilized and archived at −20 ℃. All the procedures were approved by the UST Bannu ethical committee.

Anti-acetylcholinesterase activity

AChE inhibition strength was evaluated by the methodology in Ref. [37] which was reformed by Ref. [38]. Acetylthiocholine (AcSCh) concentrations (0.05–1 mmol/L) were used in a 1 mL combination with 5,5'-dithiobis-(2-nitrobenzoic acid)) (DTNB) (10 mmol/L) and 50 mmol/L phosphate buffer (pH = 7.4) to compute hydrolysis rates (V) at 25 ℃. Further diluted snake venom (20 µL) was supplemented to the working solution and followed by 5 min incubation at 37 ℃. The reaction was started by the addition of various substrate concentrations. The reaction was examined after every 15 s for 90 s by the development of DTNB thiolate di-anion. The activity of AChE was scrutinized by the extent of the yellow color formation. The assay was performed three time to eradicate the errors. The percent inhibition was deliberated by

$$\text{Inhibition} = \frac{\text{absorbance of contral} - \text{absorbance of sample}}{\text{absorbance of contral}} \times 100\% \quad (2)$$

Protein estimation

Bradford and Thompson protocol was used to estimate the proteins [39] using bovine serum albumin as stock.

Kinetic determinations

For analyzing the type of inhibition, kinetics studies were done. The interaction of KEE, KE-AgNPs, and acetyl cholinesterase was assessed by the double reciprocal plot [34]. The reaction was assessed at different acetylthiocholine concentrations with and without KE and its NPs (10, 20, and 40 µg/mL). K_i and K_I were calculated by Cornish–Bowden plots [40] and Dixon plot [36], respectively. IC_{50} was calculated by concentration versus percent activity and percent inhibition of KEE and KE-AgNPs.

Statistical analysis

A two-way analysis of variance (ANOVA) was used for data analysis. The difference was considered to be significant at $P < 0.05$. Data was presented as mean ± standard error of the mean (SEM). The graphs were created using SlideWrite and OriginPro 8.5.

Results

UV–Vis spectroscopy of KE-AgNPs

The aqueous extract of KE was green, which changed to reddish-brown after the addition of 1 mmol/L silver nitrate ($AgNO_3$) aqueous solution and incubation for 24 h at 40 ℃. The synthesis seemed progressive, as confirmed by the color change due to the bio reduction of Ag^+ (Fig. 1).

After visual confirmation, the KE-AgNPs were exposed to UV–Vis spectral analysis at the range of 300–800 nm. Figure 2(a) represents the peak at 416 nm with absorption of 1.98, indicating the optimal conditions for KE-AgNPs biosynthesis as 24 h incubation time, 1.5 mL of aqueous extract concentration, 1 mmol/L silver nitrate solution concentration, 40 ℃, and pH = 9.

Factors affecting biosynthesis of KE-AgNPs

To standardize the nanoparticles formation route, different volumes of KE extract varied at 0.25, 0.5, 1, 1.5, and 2 mL were tested in this study, which exhibited a spectrum of absorption in the range of 300–800 nm with the increase in the intensity of peaks from 0.76 to 2.22, respectively (Fig. 2(b)).

Moreover, the UV–Vis spectra outcomes revealed a rise in the absorbance intensity of the KE-AgNPs with time (Fig. 2(c)). An absorption peak (390 nm) of very low intensity (0.79) appeared after 1 h of reaction, which transformed into a sharp and visible peak of 416 nm after 24 h and represented the formation of stable and uniform sized KE-AgNPs.

Figure 2(d) shows the temperature stability of KE-AgNPs (20–100 ℃) and suggests that a broad band of 400 nm appeared at 20 ℃. By increasing the temperature from 20 to 40 ℃, the surface plasmon resonance (SPR) band becomes sharper at 416 nm with absorption intensity of 1.98. Further, rise in temperature beyond 40 ℃ results in broadening of peaks with higher intensities of 2.24, 2.39, and 2.83 at 60, 80, and 100 ℃, respectively.

The influence of $AgNO_3$ concentration (0.5–2 mmol/L) on biogenic synthesis of KE-AgNPs synthesis was also assessed. The absorbance band of 407, 416, 403, and 411 nm appeared at 0.5, 1, 1.5, and 2 mmol/L salt concentration, respectively (Fig. 2(e)).

The effect of pH = 5–12 on the biogenic synthesis of KE-AgNPs was also evaluated (Fig. 2(f)). At pH 5 and 6, no absorption peaks appeared. But sharp SPR band of 416 nm with higher absorbance intensity (1.98) was detected as the pH was increased from 6 to 9. At higher pH beyond 9, broader peaks formed.

The stability of silver nanoparticles was studied at different time intervals of 1, 30, and 90 days. The sharp peaks at 416 nm with a maximum absorbance of 1.98 and 1.85 appeared after 24 h and 30 days, respectively, and confirmed the presence of KE-AgNPs, but after 90 days, this peak become broader with low absorbance of 0.50 (Fig. 2(g)).

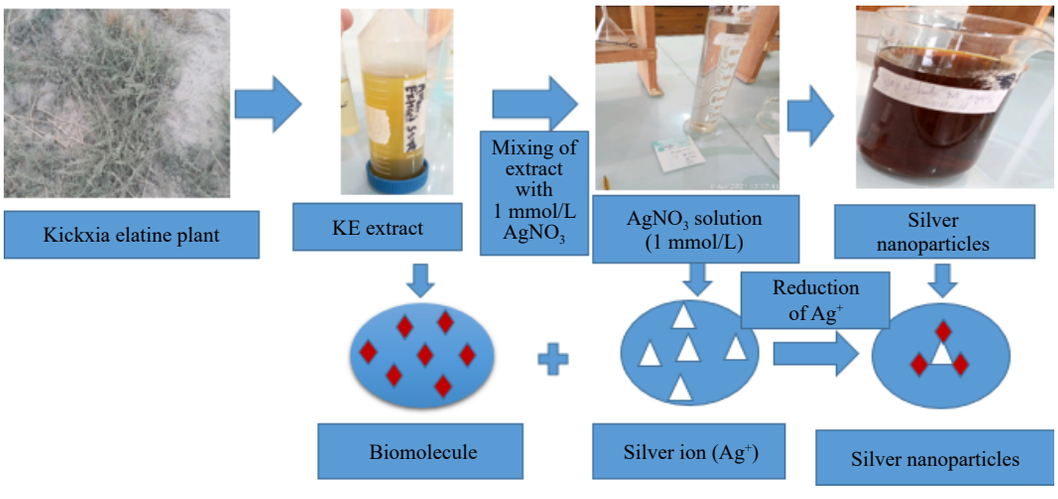


Fig. 1 Schematic presentation for the biogenic synthesis of KE-AgNPs.

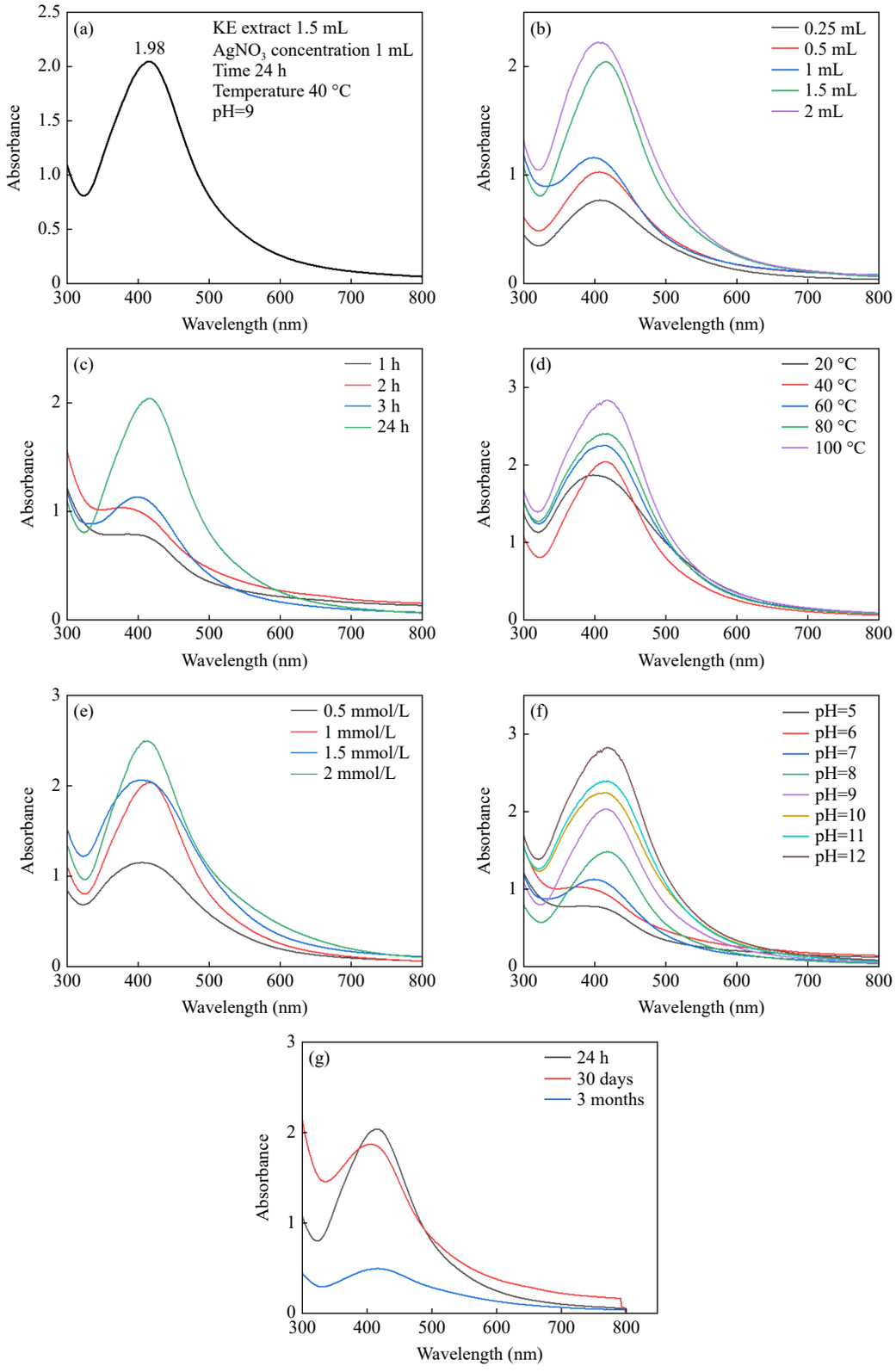


Fig. 2 (a) The UV–Vis absorption spectrum of KE-AgNPs at optimal conditions. **(b)–(g)** UV spectra of KE-AgNPs at different extract volumes, time intervals, temperatures, silver nitrate solution concentrations, pH, and stability periods, respectively.

FTIR spectroscopy of KEE and synthesized KE-AgNPs

The FTIR spectra of KE and its silver nanoparticles are displayed in Fig. 3. Various peaks were reported that attributed to the different functional groups (Table 1). The different peaks were demonstrated by KEE and KE-AgNPs in the ranges of 3 500–3 200 cm^{-1} for O—H stretch, 3 000–2 850 cm^{-1} for C—H stretch, 2 260–2 100 cm^{-1} for C≡C stretch, 2 140–1 990 cm^{-1}

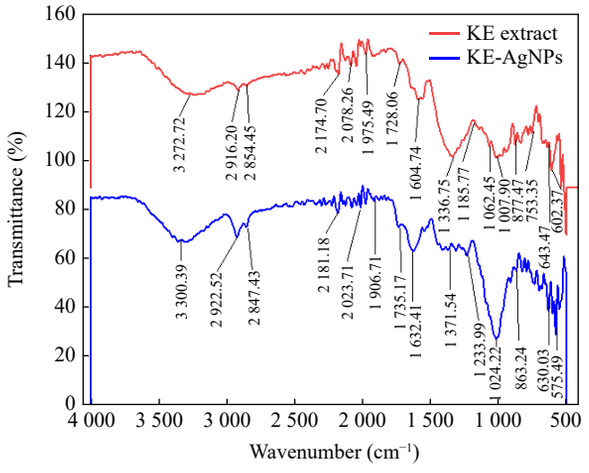


Fig. 3 FTIR analysis of KEE and KE-AgNPs.

for N—C—S stretch, 2 000–1 900 cm^{-1} for C—C—C stretch, 1 740–1 720 cm^{-1} for C—O stretch, 1 650–1 600 cm^{-1} for C—C stretch, 1 320–1 000 cm^{-1} for C—O stretch), 890–850 cm^{-1} for aromatic compounds), and 690–515 cm^{-1} for C—Br stretch.

SEM microscopy of KE-AgNPs

The nanostructure studies of size and shape elucidated by SEM are summarized in Fig. 4(a). The results specify that KE-AgNPs are mono-dispersive with uniform alignment in the matrix. Nano Measurer software was used to calculate the particle size distribution graph (Fig. 4(b)), which displayed that 90% KE-AgNPs are in an average size of 50 nm.

XRD screening of KE-AgNPs

XRD investigation of KE-AgNPs presented four strong Bragg reflections at 2θ values of 38.07°, 44.32°, 64.39°, and 77.40°, which attribute to the plane of (111), (200), (220), and (311) reflections of face-centered cubic (FCC) crystal structure of Ag (Fig. 5). The calculated full width at half maximum length (FMHM), particle size (D), interplanar d spacing, and miller constant (α) are presented in Table 2. The mean particles size of KE-AgNPs was found to be 42.47 nm using the Debye–Scherrer equation ($D = K\lambda/(\beta\cos\theta)$).

EDX screening of KE-AgNPs

EDX was used to identify the elemental components of synthesized KE-AgNPs (Fig. 6(a)). The quantitative profile of elements indicated that KE-AgNPs contain 61.67% of silver, 15.82% carbon, 15.65% oxygen, 4.93% sodium, 0.83% calcium, 0.82% chlorine, and 0.28% silicon by percent weight (Fig. 6(b)). Similarly, the elemental profile specified that KE-AgNPs contain 49% of silver, 25.41% carbon, 13.28% oxygen, 1.65% sodium, 0.34% silicon, 0.50% sulfur, 7.84% chlorine, 1.25% potassium, and 0.74% calcium by percent weight (Fig. 7(b)). The high percentage of Ag signals to KE-AgNPs.

In-vitro free radicals scavenging (antioxidant) activities

ABTS scavenging activity

In current study, KEE, KE-AgNPs, $AgNO_3$, and AA were analyzed against ABTS scavenging assay. The

Table 1 FTIR interpretation of KE extract (whole plant) and its silver nanoparticles

Serial/No.	KE Extract peak position (cm^{-1})	KE-AgNPs peak position (cm^{-1})	Corresponding frequency range (cm^{-1})	Chemical bond	Functional group
1	3 272.72	3 300.39	3 500–3 200 (s)	O—H (stretch)	Alcohol and phenol
2	2 916.20	2 922.52	3 000–2 850 (m)	C—H (stretch)	Alkanes
3	2 854.45	2 847.93	3 300–2 500 (m)	O—H (stretch)	Carboxylic acid
4	2 174.70	2 181.18	2 260–2 100 (w)	C≡C (stretch)	Alkynes
5	2 078.26	2 023.71	2 140–1 990 (s)	N=C=S (stretch)	Metal carbonyl (isothiocynate)
6	1 975.49	1 906.71	2 000–1 900 (m)	C=C=C (stretch)	Allene
7	1 728.06	1 735.17	1 740–1 720 (s)	C=O (stretch)	Conjugated Aldehyde
8	1 632.41	1 604.74	1 650–1 600 (m)	C=C (stretch)	Conjugated ketone and alkene
9	1 336.75	1 371.54	1 390–1 310 (m)	O—H (bend)	Phenols
10	1 185.77	1 233.99	1 320–1 000 (s)	C—O (stretch)	Alcohol, ester, ether, and carboxylic acid
11	1 062.45	1 024.22	1 250–1 020 (m)	C—N (stretch)	Aliphatic amines
12	877.47	863.24	890–850		Aromatic compounds
13	643.47	630.03	690–515 (s)	C—Br (stretch)	Halo compounds

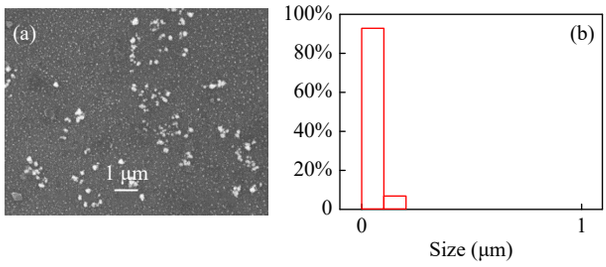


Fig. 4 (a) SEM analysis of KE-AgNPs and KE-AgNPs size demonstration by SEM. **(b)** Nano Measurer 1.2.5 was used to calculate the particle size distribution graph.

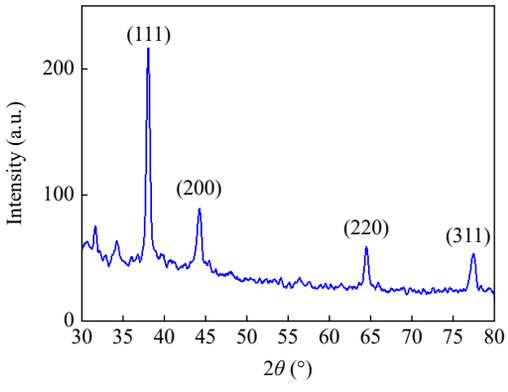


Fig. 5 XRD screening of KE-AgNPs.

scavenging activity at the four different concentrations of 40, 80, 120, and 160 μg/mL was of 28.5%, 39.3%, 49.4%, and 58.6%, and 40.2%, 51.8%, 60.9%, and 66.9% for KEE and KE-AgNPs, respectively, whereas that of $AgNO_3$ and AA was 5.83%, 8.43%, 12.4%, and 17.26%, and 45.7%, 66.8%, 77.8%, and 88.38%, respectively (Fig. 7(a)). The calculated IC_{50} values for KEE, KE-AgNPs, and AA were (124.33 ± 4.66), (77.37 ± 5.66), and (42.62 ± 7.26) μg/mL, respectively (Table 3). $AgNO_3$ does not cause 50% hunting of ABTS free radicals at any concentration.

DPPH screening assay

In recent project, KEE, KE-AgNPs, $AgNO_3$, and AA scavenging capability were evaluated against DPPH radicals. Figure 7(b) designates that at the highest concentration of 160 μg/mL, the KEE and KE-AgNPs presented the highest scavenging capacity of 66.2% and 72.49%, respectively, as compared with AA (83.36%) and $AgNO_3$ (17.53%). Table 3 indicates IC_{50} values of (82.97 ± 8.43), (44.56 ± 2.83), and (42.91 ± 1.46) μg/mL for KEE, KE-AgNPs, and AA, respectively.

Hydrogen peroxide hunting ability

In this experiment, different concentrations from 40 to 160 μg/mL of KEE, KE-AgNPs, $AgNO_3$, and AA were assessed for hydrogen peroxide hunting ability (Fig. 7(c)). At the highest concentration of 160 μg/mL, the percent scavenging activity was 60.05% ± 4.06% for KEE, 69.42% ± 0.67% for KE-AgNPs, 18.26% ± 0.73% for $AgNO_3$, and 79.04% ± 5.52% for AA, respectively. The IC_{50} values are mentioned in Table 3.

FRAP activity

In the FRAP assay (Fig. 7(d)), the reducing power of KEE, KE-AgNPs, $AgNO_3$, and AA became higher

Table 2 The grain size, interplaner spacing, and lattice constant of KE-AgNPs

Serial No.	2θ (°)	Element	*hkl*	FMHM (*β*) of intense peak (rad)	Particle size *D* (nm)	*d* spacing (Å)	Lattice constant *α* (Å)
1	38.07	Ag	111	0.003 5	40.76	2.361	4.089
2	44.32	Ag	200	0.003 3	44.71	2.041	4.083
3	64.39	Ag	220	0.003 7	37.56	1.445	4.088
4	77.40	Ag	311	0.003 0	46.84	1.231	4.084

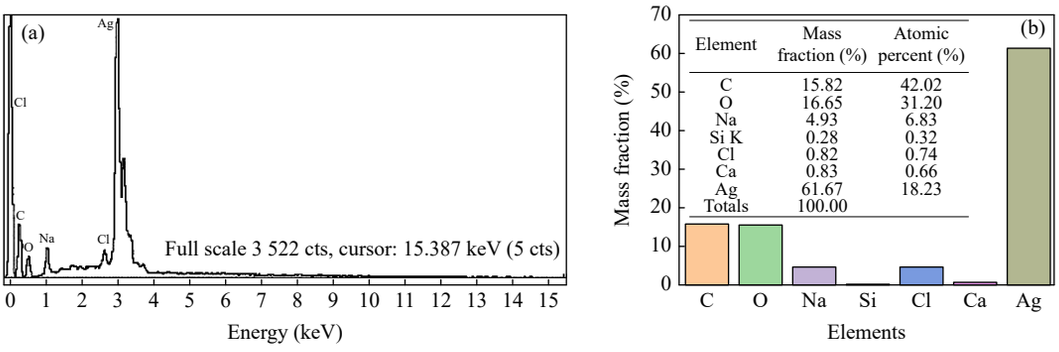


Fig. 6 (a) EDX spectrum of KE-AgNPs. **(b)** Elemental profile of biosynthesized KE-nanoparticles.

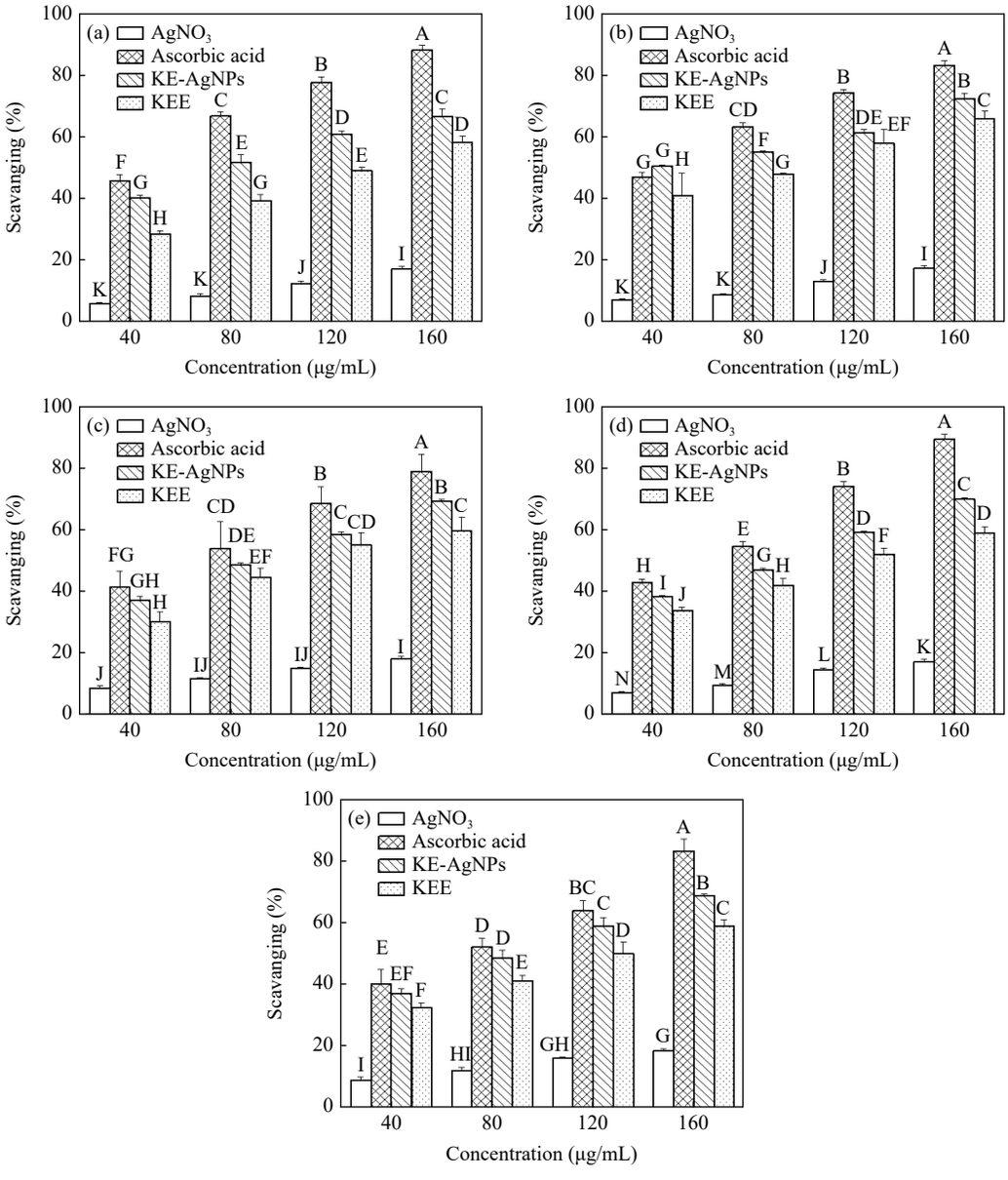


Fig. 7 (a) *In-vitro* ABTS, **(b)** DPPH, **(c)** hydrogen peroxide (H_2O_2), **(d)** FRAP, and **(e)** ammonium molybdenum antioxidant assay of KEE and KE-AgNPs. All experiments were performed in three times and data was expressed as mean ± standard deviation (SD). The capital letters represent that data was significant at $P < 0.05$.

Table 3 IC_{50} values of ascorbic acid, KE-AgNPs, and KEE in different antioxidant activities

Sample	IC_{50} (μg/mL)				
	ABTS activity	DPPH activity	H_2O_2 activity	Ferric reducing assay	Ammonium molybdenum assay
Ascorbic acid	42.62 ± 7.26	42.91 ± 1.46	64.82 ± 15.03	61.33 ± 3.88	72.19 ± 5.13
KE AgNPs	77.37 ± 5.66	44.56 ± 2.83	86.75 ± 3.42	86.17 ± 1.63	87.92± 2.72
KEExtract	124.33 ± 4.66	82.97 ± 8.43	109.92 ± 8.24	113.96 ± 2.64	119.57± 5.93

with the increase in the concentration from 40 to 160 μg/mL and displayed maximum scavenging of 59.36% ± 1.84%, 70.04% ± 0.52%, 17.2% ± 0.94%, and 89.47% ± 1.771% for KEE, KE-AgNPs, $AgNO_3$, and AA, respectively, at the highest concentration of 160 μg/mL. The IC_{50} values of all inhibitors are shown in Table 3.

Ammonium molybdenum assay

Ammonium molybdenum assay was also assessed to study the antioxidant capacity of KE-AgNPs, KEE, $AgNO_3$, and AA (Fig. 7(e)). The result depicted that at the high concentration of 160 μg/mL, KE-AgNPs exhibited increased antioxidant activity (68.77% ±

0.49%) as compared to KE extract (59% ± 1.86%), $AgNO_3$ (18.4% ± 0.73%), and AA (83.18% ± 3.98%) with IC_{50} of (119.57 ± 5.93) μg/mL for KEE, (87.92 ± 2.72) μg/mLfor KE-AgNPs, and (72.19 ± 5.13) μg/mL for AA (Table 3). $AgNO_3$ does not exhibit 50% of ammonium molybdenum scavenging potential at any concentration.

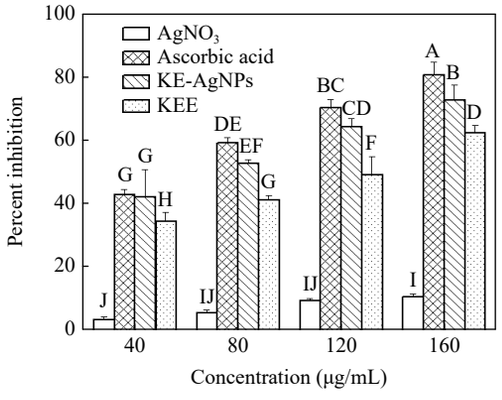


Fig. 8 Anti-alpha-amylase inhibitory capability of AgNPs, KE extract, $AgNO_3$, and glucophage. The experiments were carried out in triplicate and data was presented as mean ± SD. The capital letters represent that data was significant at $P < 0.05$.

In-vitro anti-α-amylase activity

In present study, α-amylase enzyme inhibition ability of KEE, KE-AgNPs, $AgNO_3$, and standard glucophage was evaluated. Figure 8(a) indicates that KEE, KE-AgNPs, $AgNO_3$, and glucophage repressed α-amylase action in concentration-dependent pattern. The inhibiting capacity was found to be 34.69%, 43.01%, 49.48%, and 62.75% for KEE, 42.17%, 52.72%, 64.28%, and 72.78% for KE-AgNPs, 3.53%, 5.36%, 9.63%, and 10.83% for $AgNO_3$ salt, and 42.85%, 59.18%, 70.4%, and 80.61% for glucophage at different concentrations of 25, 50, 75, and 100 μg/mL, respectively. The IC_{50} values were found to be (70.03 ± 4.04), (41.37 ± 3.90), and (35.83 ± 0.59) μg/mL for KEE, KE-AgNPs, and glucophage, respectively.

KEE and KE-AgNPs effect on V_{max} and K_m

The result showed that both KEE and KE-AgNPs inhibited α-amylase in the mixed type mode (Figs. 9(a) and 9(b)). In this type of inhibition, K_m increased (16.62%–55.45% for KEE and 49.77%–134.78% for KE-AgNPs) and V_{max} decreased (2.68%–

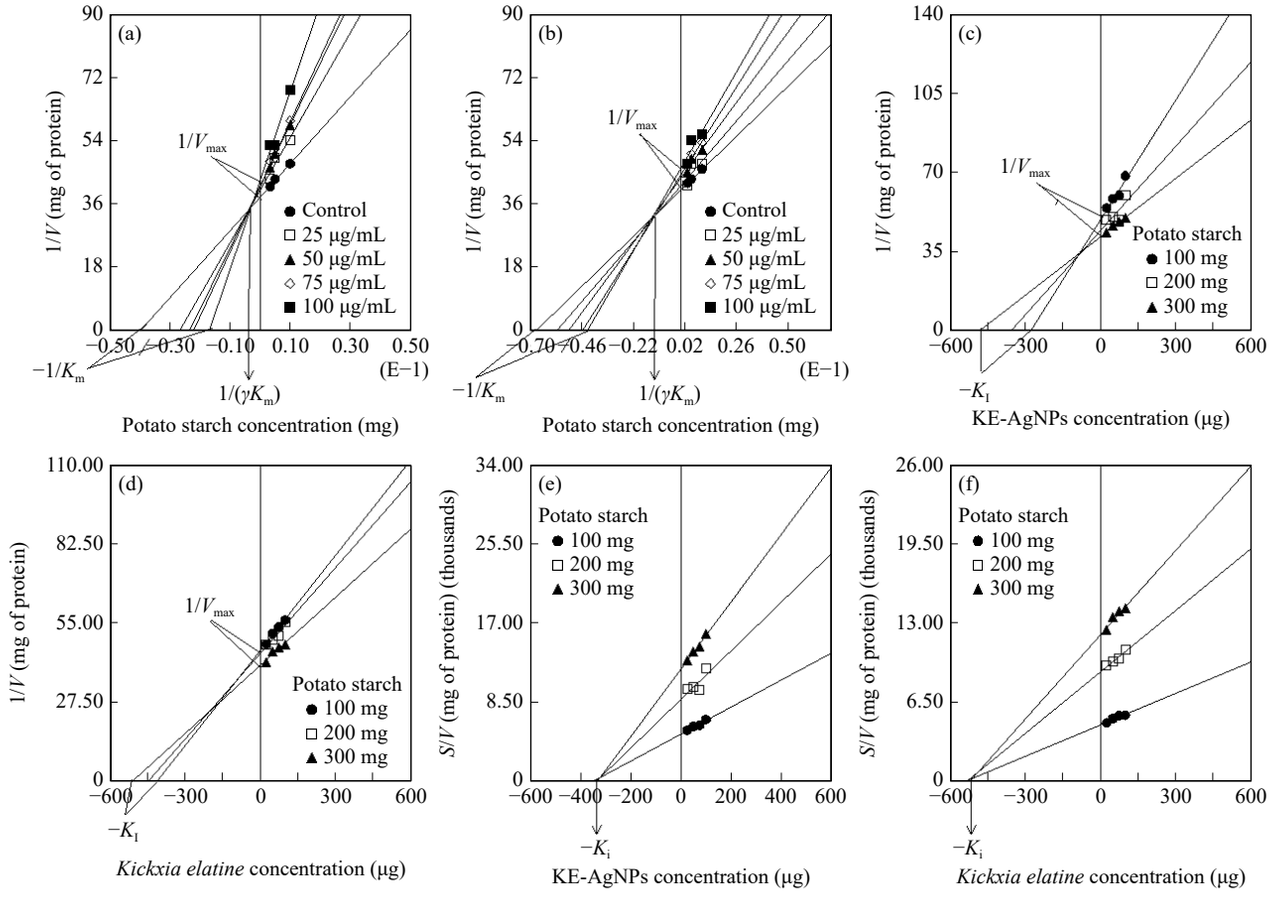


Fig. 9 (a) and **(b)** Lineweaver–Burk (reciprocal of enzyme velocity versus reciprocal of potato starch) plot representing mixed type of inhibition by KE-AgNPs and KEE. **(c)** and **(d)** Analysis of K_{Iapp} and $V_{maxiapp}$ of α-amylase. The $V_{maxiapp}$ and K_{Iapp} were calculated from Dixon plot. **(e)** and **(f)** Determination of K_i of α-amylase of KE-AgNPs and KE extract, respectively.

12.98% and 4.44%–11%), respectively, for KEE and KE-AgNPs (Table 4).

KEE and KE-AgNPs effect on K_{Iapp} and $V_{maxiapp}$ of α-amylase

Kinetics studies showed that K_{Iapp} of KEE and KE-AgNPs increased from 445.44 to 506.61 µg (9%–24%) and 355.58 to 482.66 µg (27%–73%), respectively, while $V_{maxiapp}$ values increase from 2.26% to 12.66% (for KEE) and 10.83% to 23.15% (for KE-AgNPs), respectively, with the increase in substrate concentration (Figs. 9(c) and 9(d)). The K_{Iapp} and $V_{maxiapp}$ are mentioned in Table 5.

Calculation of K_I, K_i, K_m, and γK_m of α-amylase

K_I was estimated for KEE and KE-AgNPs as 453.96 and 372.40 µg, respectively (Figs. 9(c) and 9(d)). While K_i was calculated to be 475 µg (Fig. 9(f)) and 330 µg (Fig. 9(e)) for KEE and KE-AgNPs, respectively. K_m was found to be 14.86 and 25.14 mg for KEE and KE-AgNPs, respectively. γK_m was found to be 28 and 70 mg for KEE and KE-AgNPs, respectively (Table 6).

Anti-acetylcholinesterase activity

In 1 mL assay mixture, $AgNO_3$, KEE, and KE-AgNPs exhibited 18.54% ± 0.75%, 54.78% ± 1.42%, and 63.62% ± 0.71% inhibition against snake venom AChE at the highest concentration of 40 µg/mL, respectively (Fig. 10(a)). The IC_{50} values were found to be (22.51 ± 2.91) µg/mL (KE-AgNPs) and (32.09 ± 0.29) µg/mL (KEE), as shown in Fig. 10(b).

KEE and KE-AgNPs effect on K_m and V_{max} of AChE

Kinetics studies showed that both KEE and KE-AgNPs cause mixed type of inhibition against AChE (Figs. 11(a) and 11(b)), respectively. In mixed type of inhibition, K_m increased (13.53%–101.48% and 10.10%–38.04%), while V_{max} decreased (12.66%–52.47% and 11.91%–41.69%) for KEE and KE-AgNPs, respectively (Table 7).

Effect of KEE and KE-AgNPs, on K_{Iapp} and $V_{maxiapp}$ of AChE

Kinetics studies showed that K_{Iapp} of KEE and KE-

Table 4 Effect of KEE and KE-AgNPs on K_m and V_{max} of α-amylase

Concentration (µg/mL)	Sample	V_{max}	Decrease (%)	K_m (mg)	Increase (%)
Control		0.024 96	0	14.855 6	0
25		0.024 29	2.68	17.325 5	16.62
50	KEE	0.023 07	7.57	19.232 9	29.46
75		0.022 62	9.37	21.994 7	48.05
100		0.021 72	12.98	22.944 5	54.45
Control		0.026 301	0	25.154 9	0
25		0.025 133	4.44	37.674 7	49.77
50	KE-AgNPs	0.024 35	7.41	42.580 6	69.29
75		0.024 3	7.6	44.994 2	78.86
100		0.023 41	11	59.058 8	134.78

Table 5 Effect of KEE and KE-AgNPs on K_{app} and $V_{maxiapp}$ of α-amylase

Potatostarch (mg)	Sample	K_{Iapp} (µg)	Increase (%)	$V_{maxiapp}$ (µg/(min·mg))	Increase (%)
100		409.82	0	0.022	0
200	KEE	445.44	9	0.022	2.26
300		506.61	24	0.024	12.66
100		278.95	0	0.020	0
200	KE-AgNPs	355.58	27	0.022	10.83
300		482.66	73	0.024	23.15

Table 6 Comparative study of kinetic parameters of α-amylase inhibition: K_i, K_I, K_m, IC_{50}, and γK_m of α-amylase

Sample	K_i (µg)	K_I (µg)	K_m (mg)	IC_{50} (µg/mL)	γK_m (mg)
KEE	475	453.96	14.86	70 ± 4.05	28
KE-AgNPs	330	372.40	25.14	41.38 ± 4.90	70

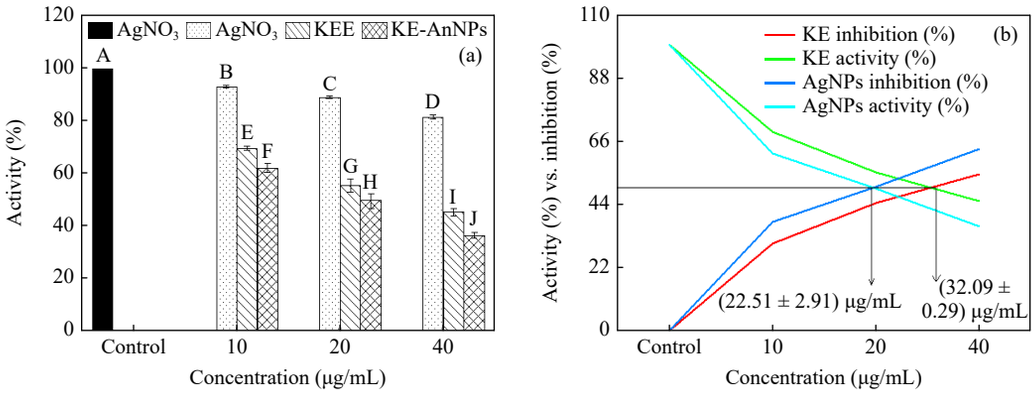


Fig. 10 (a) Inhibitory effect of $AgNO_3$, KE-AgNPs, and KEE on snake venom acetylcholinesterase enzyme. All activities were repeated three time to eliminate the errora and data was represented as an average of the three experiments. Data was significant at $P < 0.05$. (b) IC_{50} values of KE-AgNPs and KEE that produce 50% inhibition of AchE.

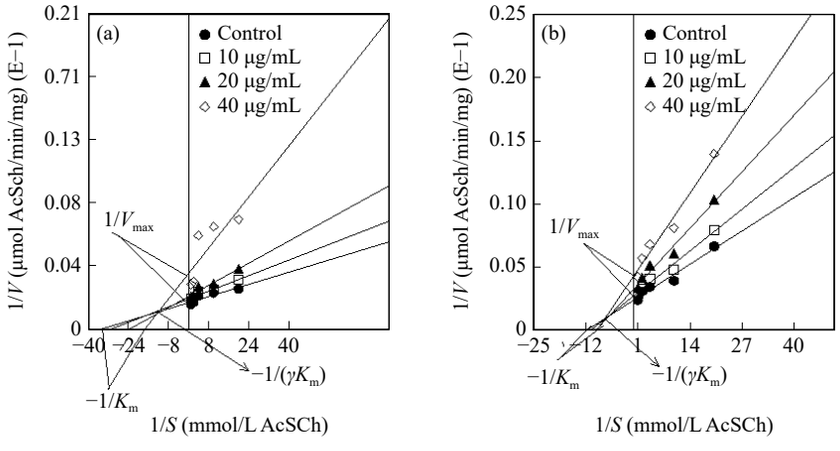


Fig. 11 Lineweaver–Burk plot showing mixed type of inhibition caused by **(a)** KEE and **(b)** KE-AgNPs, respectively.

Table 7 Effect of KEE and KE-AgNPs on K_m and V_{max} of AChE

Concentration (μg/mL)	Sample	V_{max} (μg/(min·mg))	Decrease (%)	K_m (mmol/L)	Increase (%)
Control	KEE	566.251 415 6	0	0.028 315	0
10		494.559 841 7	12.66	0.032 146	13.53
20		459.981 600 7	18.76	0.042 318	49.45
40		269.106 566 2	52.47	0.057 050	101.48
Control	KE-AgNPs	422.654 268 8	0	0.086 221	0
10		372.300 819 6	11.91	0.094 936	10.10
20		305.343 511 4	27.75	0.105 038	21.82
40		246.426 812 3	41.69	0.119 024	38.04

AgNPs increased from 20.65 to 40.68 μg and from 34.77 to 40.26 μg, respectively. The $V_{maxiapp}$ values also increased from 7% to 16.43% and from 62% to 173% for KEE and KE-AgNPs, respectively, with the increase in substrate concentration (Table 8). K_{Iapp} and $V_{maxiapp}$ values were calculated from Figs. 12(a) and 12(b) for KEE and KE-AgNPs, respectively.

Determination of K_I, K_i, γK_m, *and* K_m

The K_I was estimated for KEE and KE-AgNPs as 27.93 and 35.96 μg, respectively (Figs. 12(a) and 12(b)). While K_i was found to be 40 μg (Fig. 13(a)) and 33.3 μg (Fig. 13(b)) for KEE and KE-AgNPs, respectively. The γK_m was found to be 0.06 and 0.11 mmol/L for KEE and KE-AgNPs, respectively. The

K_m was determined as 0.03 and 0.08 mmol/L for KEE and KE-AgNPs, respectively (Table 9).

Table 8 Effect of KEE and KE-AgNPs on K_{Iapp} and $V_{maxiapp}$ of AChE

AcSch (mmol/L)		K_{Iapp} (mmol/L)	Increase (%)	$V_{maxiapp}$ (μg/(min·mg))	Increase (%)
0.05		14.17	0	555.55	0
0.1		20.65	46	597.73	7
0.25	KEE	23.47	66	608.64	9.56
0.5		40.56	186	632.11	13.78
1		40.68	187	646.83	16.43
0.05		31.21	0	162.63	0
0.1		34.77	11	263.85	62
0.25	KE-AgNPs	34.99	12	314.07	93
0.5		38.57	24	375.79	131
1		40.26	29	443.45	173

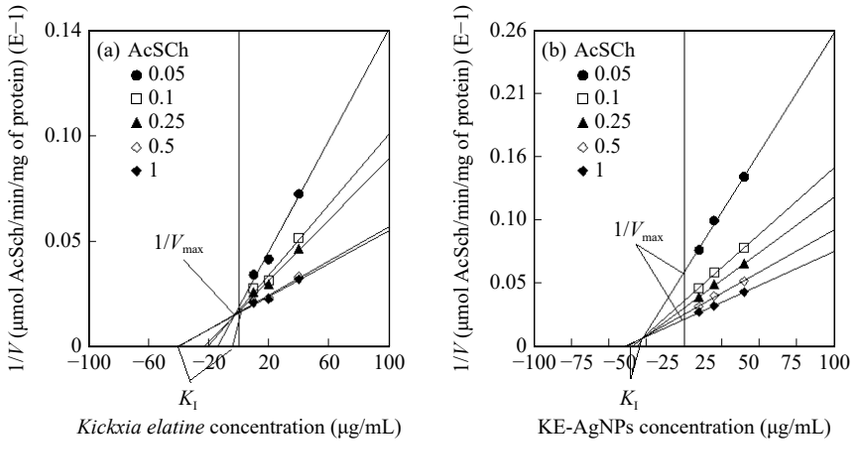


Fig. 12 Determination of K_{Iapp} and $V_{maxiapp}$ for (a) KEE and (b) KE-AgNPs using Dixon plot for AchE.

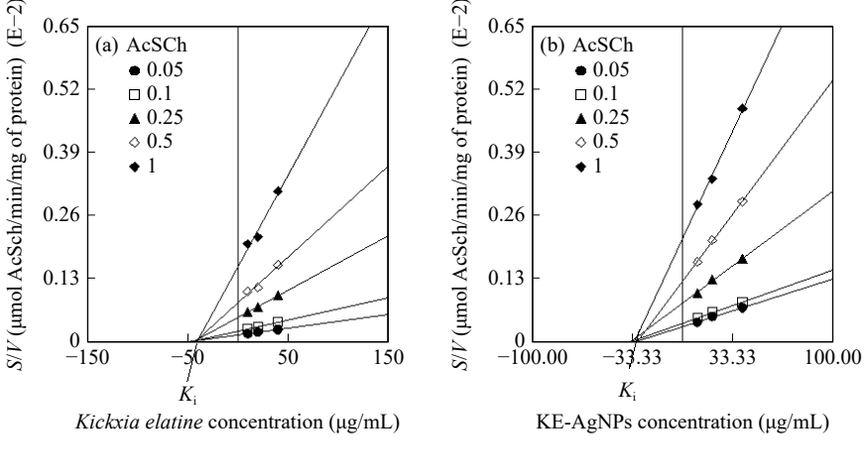


Fig. 13 Determination of K_i for **(a)** KEE and **(b)** KE-AgNPs using Cornish–Bowden plots for AchE.

Table 9 Comparative study of kinetic parameters of AChE inhibition: K_i, K_I, K_m, IC_{50}, and γK_m values

Sample	K_i (μg)	K_I (μg)	K_m (mmol/L)	IC_{50} (μg/mL)	γK_m (mmol/L)
KEE	40	27.93	0.03	32.09 ± 0.286	0.06
KE-AgNPs	33.3	35.96	0.08	22.51 ± 2.906	0.11

Discussion

The UV spectroscopy technique is used to analyze the formation of different size NPs [41]. Bio-mediators existing in the extract reduced and stabilized Ag^+, due to the changes in the SPR of metal nanoparticles [42]. In current study, when a solution of 1.5 mL of KEE and 1 mmol/L silver nitrate was incubated at 40 ℃ for 24 h and adjusted the pH to 9, the synthesis of AgNPs seemed progressive, as confirmed by the color change from green to reddish-brown due to the bio-reduction of Ag^+ by the phyto-components present in KE aqueous extract. Metal-based NPs have many free electrons (e^-). The excitation of free e^- displayed the SPR effect with the light of specific wavelengths [43]. In present study, the sharp peak was documented at 416 nm at higher absorption of 1.98. A similar absorbance peak at 420 nm was described by Naghmouchi et al., in AgNPs synthesized from *Mentha pulegium* leaves [44].

Fabrication of the AgNPs is affected by various parameters (extract volume, temperature, time, $AgNO_3$ concentration, and pH) [45]. To standardize the nanoparticles formation route, KE-AgNPs were produced under various circumstances such as KEE volume, temperature, time, $AgNO_3$ salt concentration, and pH. In the present report, the increase in volume of KE extract corresponds to the increase in the intensity of peaks. The SPR at a lower volume of 0.25 mL was broad and became sharper with the increase of the KE extract volume. The higher bandwidth at lower volume corresponds to formation of large anisotropic AgNPs, because the quantity of phytochemicals (phenols, flavonoids, saponin, alkaloids, tannins, and proteins) reduces with the drop of the volume of extract. At optimal volume of 1.5 mL, the sharp band at 416 nm attributes to fabrication of small and isotropic particles. These investigations are related to earlier reports of Amin et al., and suggested that the increase in *Solanum xanthocarpum* extract volume correlated positively with stability of AgNPs [46]. Higher absorbance intensity of 2.21 was reported on further increase in KE extract volume to 2 mL and violet beer and lambert law. An ideal and definite incubation time is required for thorough reaction of Ag ion with active biomolecules present in plant extract. Thus, in current study, the impact of incubation period on biosynthesis of KE-AgNPs was also assessed. The results revealed that absorbance intensity of the KE-AgNPs increases with reaction time. After 1 h of reaction, an absorption peak of 390 nm appeared very low intensity, which transformed into a sharp and visible peak of 416 nm after 24 h, representing the formation of stable and spherical KE-AgNPs. Thus the optimum time required for complete reduction of Ag^+ was recorded to be 24 h. Awwad and Salem reported the optimum reaction time of 60 min for synthesis of stable mulberry leaves extract based on AgNPs [47].

For the production of small and active AgNPs, an ideal temperature is needed. In the current report, the effect of temperature on formation of KE-AgNPs was also evaluated and outcomes showed that the SPR peaks became sharper by increasing the temperature from 20 to 40 ℃. At 40 ℃, the sharp absorption band at 416 nm indicated the development of stable, small, and uniform sized KE-AgNPs. Further increase in temperature to 100 ℃ resulted in broadening of peaks and revealed the increase in size of NPs. The AgNPs tend to be unstable with the increase in temperature beyond 40 ℃ [48]. In current study, various concentrations of $AgNO_3$ were tested for synthesis of KE-AgNPs, while retaining all the other parameters constant. The results revealed that the lower concentration of 0.5 mmol/L silver nitrate was deficient for fabrication of NPs, but at elevated concentration (1.5–2 mmol/L), KE-AgNPs mixture became foggy due to the reaction of excessive $AgNO_3$ with phytochemicals, subsequently resulted in broad peaks. The broad peak indicates large-sized NPs. The results are in good agreement with reports present in Ref. [49]. The broad peak indicates large-sized NPs. Kaya et al. reported that small nanometer-sized NPs are biologically more active [50]. The KE-AgNPs produced from 1 mmol/L silver nitrate concentration displayed sharp peak at 416 nm, which designated biologically active small size NPs.

For biogenic synthesis of AgNPs, a specific pH is required [51]. Therefore, in the recent project, the pH effect on the biosynthesis of KE-AgNPs was also evaluated. All experiments were carried out by varying the pH (5–12), while keeping all the other parameters constant. At pH 5 and 6, no absorption peaks appeared. But sharp bands were detected as the pH was increased from 6 to 9 and conferred biosynthesis of isotropic and stable KE-AgNPs. At higher pH beyond 9, the formation of broader peaks indicates large size NPs. Thus pH study showed that the fabrication of AgNPs is enhanced by basic

conditions while repressed by acid conditions [52].

The biological efficacy of the AgNPs is greatly dependent on their stability. Every type of metal NPs has an optimum stability period after which its strength and efficacy are reduced or diminished. In this work, the stability of the KE-AgNPs was monitored at various periods of 1, 30, and 90 days. The characteristic SPR bands at 416 and 408 nm with absorbance peaks of 1.98 and 1.85 after 1 and 30 days confirmed the NPs stability. But after 3 months, the SPR band became broader with low absorbance of 0.50 and showed that KE-AgNPs lost their stability. Similar results were reported by Ref. [53], who synthesized grape juice-based AgNPs and stated that during 30 days, no alteration in the shape, position, and symmetry of the SPR absorption peak takes place.

FTIR measurement was carried out in order to reveal the possible biomolecules which is accountable for the reduction of Ag^+ and its interaction with the stabilization and capping of AgNPs. The phytochemicals present on surface of KE-AgNPs were inspected by comparing IR spectra of KEE and KE-AgNPs. The different peaks in FTIR spectroscopy indicate the existence of phenolic, alcoholic, aromatic, carbonyl compounds of the protein, alkynes, conjugated aldehydes, ester, ether, carboxylic acid, aliphatic amines, and halo compounds in KEE and KE-AgNPs. The phenolic and alcoholic compounds are good stabilizing agents to reduce AgNPs [54]. The carbonyl compounds of proteins contribute to the stabilization of KE-AgNPs by capping them [55]. The FTIR spectra of KE-AgNPs with the significant lowering in intensity attributed to interaction between KE extract and KE-AgNPs. Thus, from the IR spectrum, it may be assumed that these biomolecules are involved in the bioreduction as well as in the stabilization of KE-AgNPs [56].

The morphological studies of size and shape were interpreted by SEM and showed that KE-AgNPs are mono-dispersive with uniform alignment in the matrix. The grain sizes of the NPs valued from the SEM (50 nm) are comparable to XRD data (42.47 nm). The results are consistent with an earlier report in which AgNPs synthesized using *Morus alba* leaf are spherical with size ranging below 50 nm [57].

XRD investigation of KE-AgNPs presented the four strong Bragg reflections that correspond to the pure silver metal with FCC symmetry with an average size of 42.47 nm. These outcomes are supported by the previous literature [48], where Ag-NPs synthesized from *Euphorbia serpens* were FCC crystals of 50 nm size and similar diffraction planes were observed. Singh et al. [58] reported that *Carissa carandas* L. leaf synthesized AgNPs are crystalline with crystallite size of 35 nm.

EDX analysis gives information concerning the participation of elements in the reduction of Ag^+ both qualitatively and quantitatively [59]. The quantitative profile of elements indicated that KE-AgNPs contain appreciable and high percentage of silver, followed by carbon, oxygen, sodium, calcium, chlorine, and silicon. The silver showed a high intensity peak at 3 keV due to SPR and confirmed the complete reduction of Ag^+ to AgNPs [60]. The presence of carbon and oxygen corresponds to an aromatic compound that gives stability to reduce Ag [61]. The fluctuated percentage of carbon may be due to the carbon tape used to fasten the samples to the sample holder [62].

Oxidative stress is caused by electron deficient free radicals and linked with many disorders such as diabetes, cancer, neurological disorders, Parkinson's disease, and cognitive impairment [63]. Antioxidants are substances that lower the oxidative stress by scavenging free radicals. Therefore, antioxidant capabilities of KEE and KE-AgNPs were investigated to minimize the effect of oxidative stress. KEE and KE-AgNPs were analyzed against ABTS and showed potential scavenging activity with smaller IC_{50} values. The increasing trend in scavenging activity of KE-AgNPs can be credited to their specific shape and small size due to which they became more sensitive as compared with KEE [64].

For assessing the free-radical terminating strength of various compounds, DPPH radical scavenging capability is used [65]. DPPH radical scavenging capacity of KE and KE-AgNPs was measured by alteration in color. The change in the color was noticed due to the contribution of the hydrogen atom and electron by NPs to stable the DPPH molecule [66]. In current research, the KE and KE-AgNPs presented the highest DPPH scavenging potential. A similar finding was described by Gaber et al., in extracts from pomegranate and guava residues [67]. The outstanding potential in scavenging activity of

AgNPs might be attributed to the interference of phenolic-rich content of the extract in the stabilization and capping of NPs [68].

H_2O_2 is the main reactive oxygen species, due to its capacity to alter toxic to hydrophilic and converted to hydroxyl radical in the cell and damage the cell membrane [69]. In this experiment, different concentrations of KE and KE-AgNPs were tested for hydrogen peroxide hunting ability. The results revealed that the percent scavenging activity of KE extract and KE-AgNPs increases in positive trend with increasing the concentration and is supported by Mata et al., who used leaf extract of *Abutilon indicum* for biosynthesis of AgNPs and found that these NPs exhibits a good free radical inhibition activity [70].

In the FRAP assay, the reducing power of KEE, KE-AgNPs, and ascorbic acid became higher with the increase in the concentration in a dose-dependent manner. KE-AgNPs exhibited high inhibitory potential (IC_{50} = (86.17 ± 1.63) μg/mL) as compared with KEE (IC_{50} = (113.96 ± 2.64) μg/mL). The higher FRAP activity of KE-AgNPs was due to the phytochemicals encapsulation on the AgNPs surface [71]. Similar outcomes were described with mango leaf extract assisted AgNPs [72].

Ammonium molybdenum activity was also assessed to study the antioxidant capacity of KE-AgNPs and KEE. The result depicted that KE-AgNPs exhibited higher antioxidant activity than KEE and lower activity as compared with AA. Our results are related to an earlier report, in which AgNPs synthesized using *Calligonum polygonoides* extract exhibited a higher antioxidant capacity [28]. The presence of alkaloids, phenols, and flavonoids enhances KE-AgNPs activity by diffusion into metal Ag [14].

Carbohydrates, proteins, and fat metabolism are associated with insulin, and lack of insulin results in a disturbance of electrolyte and water homeostasis [73]. The eznyme α-amylase plays an important role in carbohydrate degradation. Therefore, suppressing the enzymatic activity of α-amylase could minimize carbohydrates degradation, which would, in turn, reduce the absorption of glucose, therefore lowering the postprandial blood glucose level [33]. Synthetic α-amylase inhibitor causes complications like diarrhea, abdominal pain, and soft feces in the colon. Therefore, Ayurvedic systems moved towards the alternative which does not bear adverse effects in addition to the insulin property [74]. So this study on the anti-diabetic properties was conducted in which α-amylase inhibition showed a good response. The phytochemicals like tannins, alkaloids, carbohydrates, terpenoids, steroids, and flavonoids found in extract and biosynthesized AgNPs are novel sources for the development of new types of anti-hyperglycemic molecules [75]. In current study, KE-AgNPs show higher anti-diabetic bioactivity as compared with KEE. This is because higher surface-to-volume ratios attribute to more surface area for electron transfer reaction and more activity [76].

In our current finding, mixed type inhibition was observed against α-amylase for both KEE and KE-AgNPs (K_m increased and V_{max} decreased). A similar result was reported previously by Shah et al. using *Silene arenosa* extracts [77]. The nanoparticles bind to other sites instead of the active site such as the peripheral binding site (P-site) [78]. Consequently, we recommend the following interactional patterns

$$\alpha\text{-amylase} + K.\ elatine \Leftrightarrow \alpha\text{-amylase}.\ K.\ elatine$$

$$\alpha\text{-amylase}.\ K.\ elatine + S \Leftrightarrow \alpha\text{-amylase}.\ K.\ elatine.\ \text{Potato starch}$$

$$\alpha\text{-amylase}.\ K.\ elatine.\ S \Leftrightarrow \alpha\text{-amylase}.\ \text{Potato starch} + K.\ elatine$$

$$\alpha\text{-amylase}.\ S \text{ and } \alpha\text{-amylase}.\ K.\ elatine.\ S \Leftrightarrow \alpha\text{-amylase}.\ P$$

$$\alpha\text{-amylase}.\ P \Leftrightarrow \alpha\text{-amylase} + P$$

Both binary (α-amylase. *K. elatine* or α-amylase. P) and tertiary (α-amylase. *K. elatine*. S) complexes could be formed. In mixed inhibition type, the complex (α-amylase. *K. elatine*. S) releases the product slowly and reduces the V_{max}. Thus, the plant and KE-mediated AgNPS may be a potential source of new herbal medicine for diabetes-II and α-amylase inhibitors kinetic studies could be convenient for new diabetes-II purposes.

Alzheimer's disease (AD) occurs due to a low level of the neurotransmitter acetylcholine [79]. Recently, the primary approach to boosting the level of AcSCh in Alzheimer's patients is to suppress the activity of AChE. The enzyme AChE catalyzes the hydrolysis of AcSCh after its liberation at the cholinergic synapses to return to its resting state after activation [80]. The effect of silver ions and AgNPs against AChE was revealed by *in vitro* studies [81]. The release of Ag^+

ion by AgNPs due to surface oxidation might be the possible mode of action as it increases interaction with AChE and subsequently inhibits its activity [82]. Currently, we confirmed the repression of krait (*B. sindanus*) venom AChE by KE extract and KE-AgNPs and found that at a fixed 0.5 mmol/L concentration of substrate, KEE and KE-NPs exhibited 50% inhibition at a concentration of 32.09 and 22.51 μg/mL, respectively. Kinetic studies discovered that KEE and KE-AgNPs presented an upsurge in the K_m with a decrease in the V_{max} and confirmed mixed-type inhibition against AChE. In this type of inhibition, AgNPs have the capability to bind to AChE and the enzyme-substrate (AChE-AcSCh) complex [83]. The inhibition of *Bungarus sindus* venom AChE positively correlated with the concentration of KE-AgNPs. These results are supported by earlier studies, in which AChE inhibition percentage increases positively with the increase in *S. arenosa* extract concentration [84].

Conclusion

KE extract has been successfully utilized for the production of simple, quick, and stable silver nanoparticles. The KE-AgNPs bio-fabrication depends on silver salt, pH, reaction time, temperature, and extract concentration. Furthermore, KE-AgNPs characterization was done by UV–Vis spectroscopy, EDX, SEM, FTIR, and XRD analyses. KE-AgNPs were also scrutinized for their biological properties and revealed greater anti-α amylase, antioxidant, and anti-AChE activities in comparison to KEE. Therefore, this study may lead to the conclusion that KE-AgNPs can be employed as an alternative option against diseases related to free radicals.

CRediT Author Statement

Noor Ul Huda: Original article writing. **Mushtaq Ahmad**: Supervision. **Nadia Mushtaq**: Data curation. **Rahmat Ali Khan**: Methodology.

Conflict of Interest

The authors declare no conflicts of interest regarding the content of this article.

References

[1] R. Kumar, G. Ghoshal, A. Jain, et al. Rapid green synthesis of silver nanoparticles (AgNPs) using (prunus persica) plants extract: Exploring its antimicrobial and catalytic activities. *Journal of Nanomedicine & Nanotechnology*, 2017, 8(4): 1000452. https://doi.org/10.4172/2157-7439.1000452

[2] S. Parmar, H. Kaur, J. Singh, et al. Recent advances in green synthesis of Ag NPs for extenuating antimicrobial resistance. *Nanomaterials*, 2022, 12(7): 1115. https://doi.org/10.3390/nano12071115

[3] H. Kumar, K. Bhardwaj, K. Kuča, et al. Flower-based green synthesis of metallic nanoparticles: Applications beyond fragrance. *Nanomaterials*, 2020, 10(4): 766. https://doi.org/10.3390/nano10040766

[4] S.S. Dash, J. Banerjee, S. Samanta, et al. Microwave-assisted fabrication of silver nanoparticles utilizing seed extract of *Areca catechu* with antioxidant potency and evaluation of antibacterial efficacy against multidrug resistant pathogenic bacterial strains. *BioNanoScience*, 2022, 12(1): 210−227. https://doi.org/10.1007/s12668-021-00927-1

[5] A.A.H. Abdellatif, S.S. Alhathloul, A.S.M. Aljohani, et al. Green synthesis of silver nanoparticles incorporated aromatherapies utilized for their antioxidant and antimicrobial activities against some clinical bacterial isolates. *Bioinorganic Chemistry and Applications*, 2022, 2022: 2432758. https://doi.org/10.1155/2022/2432758

[6] M. Vanin dos Santos Lima, G. Beloni de Melo, L. Gracher Teixeira, et al. Green synthesis of silver nanoparticles using Ilex paraguariensis extracts: Antimicrobial activity and acetilcolinesterase modulation in rat brain tissue. *Green Chemistry Letters and Reviews*, 2022, 15(1): 128−138. https://doi.org/10.1080/17518253.2021.2024896

[7] S. Majeed, M. Danish, N.A. Zakariya, et al. *In vitro* evaluation of antibacterial, antioxidant, and antidiabetic activities and glucose uptake through 2-NBDG by hep-2 liver cancer cells treated with green synthesized silver nanoparticles. *Oxidative Medicine and Cellular Longevity*, 2022, 2022: 1–14. https://doi.org/10.1155/2022/1646687

[8] M. Liu, Q. Huang, Y. Zhu, et al. Harnessing reactive oxygen/nitrogen species and inflammation: Nanodrugs for liver injury. *Materials Today Bio*, 2022, 13: 100215. https://doi.org/10.1016/j.mtbio.2022.100215

[9] T. Zhao, W. Wu, L. Sui, et al. Reactive oxygen species-based nanomaterials for the treatment of myocardial ischemia reperfusion injuries. *Bioactive Materials*, 2022, 7: 47−72. https://doi.org/10.1016/j.bioactmat.2021.06.006

[10] S. Saqib, A. Nazeer, M. Ali, et al. Catalytic potential of endophytes facilitates synthesis of biometallic zinc oxide nanoparticles for agricultural application. *BioMetals*, 2022, 35(5): 967−985. https://doi.org/10.1007/s10534-022-00417-1

[11] N. Sher, M. Ahmed, N. Mushtaq, et al. Hippeastrum hybridum assisted bioreduction of Hydrogen tetrachloroaurate (III) trihydrate: Multifaced application. 2022. https://doi.org/10.21203/rs.3.rs-1639345/v1

[12] L. Farhadi, M. Mohtashami, J. Saeidi, et al. Green synthesis of chitosan-coated silver nanoparticle, characterization, antimicrobial activities, and cytotoxicity analysis in cancerous and normal cell lines. *Journal of Inorganic and Organometallic Polymers and Materials*, 2022, 32(5): 1637−1649. https://doi.org/10.1007/s10904-021-02208-6

[13] M. Binsalah, S. Devanesan, M.S. AlSalhi, et al. Biomimetic synthesis of silver nanoparticles using ethyl acetate extract of urtica diocia leaves; characterizations and emerging antimicrobial activity. *Microorganisms*, 2022, 10(4): 789. https://doi.org/10.3390/microorganisms10040789

[14] S. Bawazeer, A. Rauf, S.U.A. Shah, et al. Green synthesis of silver nanoparticles using *Tropaeolum majus*: Phytochemical screening and antibacterial studies. *Green Processing and Synthesis*, 2021, 10(1): 85−94. https://doi.org/10.1515/gps-2021-0003

[15] M.J. Ahmed, G. Murtaza, A. Mehmood, et al. Green synthesis of silver nanoparticles using leaves extract of *Skimmia laureola*: Characterization and antibacterial activity. *Materials Letters*, 2015, 153: 10−13. https://doi.org/10.1016/j.matlet.2015.03.143

[16] A. Verma, M.S. Mehata. Controllable synthesis of silver nanoparticles using Neem leaves and their antimicrobial activity. *Journal of Radiation Research and Applied Sciences*, 2016, 9(1): 109−115. https://doi.org/10.1016/j.jrras.2015.11.001

[17] F. Zamarchi, I.C. Vieira. Determination of paracetamol using a sensor based on green synthesis of silver nanoparticles in plant extract. *Journal of Pharmaceutical and Biomedical Analysis*, 2021, 196: 113912. https://doi.org/10.1016/j.jpba.2021.113912

[18] M. Khan, F. Hussain, S. Musharaf. Preliminary floristic range of Tehsil Takht-e-Nasrati Pakistan. *International Journal of Biosciences*, 2012, 1(6): 88–99.

[19] M.P. Yuldashev, V.M. Malikov, É. K. Batirov. Flavonoids of the epigeal part ofKickxia elatine. *Chemistry of Natural Compounds*, 1996, 32(1): 30−32. https://doi.org/10.1007/BF01373784

[20] T. Cheriet, B. Ben-Bachir, O. Thamri, et al. Isolation and biological properties of the natural flavonoids pectolinarin and pectolinarigenin—a review. *Antibiotics*, 2020, 9(7): 417. https://doi.org/10.3390/antibiotics9070417

[21] B.I. Patel, P.D. Sachdeva. Anti-diabetic activity of Linaria ramosissima (WALL) Janch in streptozotocin induced diabetic rats. *International Journal of Pharmacy and Pharmaceutical Sciences*, 2014, 6: 166−171.

[22] B.H. Havsteen. The biochemistry and medical significance of the flavonoids. *Pharmacology & Therapeutics*, 2002, 96(2/3): 67–202. https://doi.org/10.1016/S0163-7258(02)00298-X

[23] P. Pandya, H. Aghera, B.K. Ashok, et al. Diuretic activity of Linaria ramosissima (wall.) Janch. leaves in albino rats. *AYU* (*an International Quarterly Journal of Research in Ayurveda*), 2012, 33(4): 576. https://doi.org/10.4103/0974-8520.110517

[24] A. Jain, S.S. Katewa, P. Galav, et al. A. Some therapeutic uses of biodiversity among the tribals of Rajasthan. *Indian Journal of Traditional Knowledge*, 2008, 7(2): 256−262.

[25] A. Amin, E. Tuenter, K. Foubert, et al. *In vitro* and in silico antidiabetic and antimicrobial evaluation of constituents from kickxia ramosissima (nanorrhinum ramosissimum). *Frontiers in Pharmacology*, 2017, 8: 232. https://doi.org/10.3389/fphar.2017.00232

[26] C. Rank, L.S. Rasmussen, S.R. Jensen, et al. Cytotoxic constituents of Alectra and Striga species. *Weed Research*, 2004, 44(4): 265−270. https://doi.org/10.1111/j.1365-3180.2004.00398.x

[27] A. Venditti, C. Frezza, I. Serafini, et al. Iridoids of chemotaxonomy relevance, a new antirrhinoside ester and other constituents from *Kickxia spuria* subsp. integrifolia (brot.) R.Fern. *Chemistry & Biodiversity*, 2018, 15(2): e1700473. https://doi.org/10.1002/cbdv.201700473

[28] N. Sher, M. Ahmed, N. Mushtaq, et al. *Calligonum polygonoides* reduced nanosilver: A new generation of nanoproduct for medical applications. *European Journal of Integrative Medicine*, 2020, 33: 101042. https://doi.org/10.1016/j.eujim.2019.101042

[29] M.A. Gyamfi, M. Yonamine, Y. Aniya. Free-radical scavenging action of medicinal herbs from Ghana. *General Pharmacology*: *the Vascular System*, 1999, 32(6): 661−667.

[30] E. Pick, D. Mizel. Rapid microassays for the measurement of superoxide and hydrogen peroxide production by macrophages in culture using an automatic enzyme immunoassay reader. *Journal of Immunological Methods*, 1981, 46(2): 211−226. https://doi.org/10.1016/S0306-3623(98)00238-9

[31] M. Oyaizu. Studies on products of browning reaction. Antioxidative activities of products of browning reaction prepared from glucosamine. *The Japanese Journal of Nutrition and Dietetics*, 1986, 44(6): 307−315. https://doi.org/10.5264/eiyogakuzashi.44.307

[32] D. Ahmed, M. Khan, R. Saeed. Comparative analysis of phenolics, flavonoids, and antioxidant and antibacterial potential of methanolic, hexanic and aqueous extracts from adiantum caudatum leaves. *Antioxidants*, 2015, 4(2): 394−409. https://doi.org/10.3390/antiox4020394

[33] M.B. Narkhede, P.V. Ajimire, A.E. Wagh, et al. *In vitro* antidiabetic activity of Caesalpina digyna (R.) methanol root extract. *Asian Journal of Plant Science and Research*, 2011, 1(2): 101–106.

[34] H. Lineweaver, D. Burk. The determination of enzyme dissociation constants. *Journal of the American Chemical Society*, 1934, 56(3): 658−666. https://doi.org/10.1021/ja01318a036

[35] B.H.J. Hofstee. On the evaluation of the constants V_m and K_M in enzyme reactions. *Science*, 1952, 116(3013): 329−331. https://doi.org/10.1126/science.116.3013.329

[36] M. Dixon, E. Webb. Determination of inhibitor constants. *Enzymes*, 1964: 328–330.

[37] M. Ahmed, J.B.T. Rocha, C. Mazzanti, et al. Comparative study of the inhibitory effect of antidepressants on cholinesterase activity in *Bungarus sindanus* (krait) venom, human serum and rat striatum. *Journal of Enzyme Inhibition and Medicinal Chemistry*, 2008, 23(6): 912−917. https://doi.org/10.1080/14756360701809977

[38] J.B. Rocha, T. Emanuelli, M.E. Pereira. Effects of early undernutrition on kinetic parameters of brain acetylcholinesterase from adult rats. *Acta Neurobiologiae Experimentalis*, 1993, 53(3): 431−437.

[39] D.S. Bradford, R.C. Thompson. Fractures and dislocations of the spine. Indications for surgical intervention. *Minnesota Medicine*, 1976, 59(10): 711−720.

[40] M.L. Cárdenas, A. Cornish-Bowden, T. Ureta. Evolution and regulatory role of the hexokinases. *Biochimica et Biophysica Acta* (*BBA*) *-Molecular Cell Research*, 1998, 1401(3): 242–264. https://doi.org/10.1016/S0167-4889(97)00150-X

[41] S. Shrivastava, D. Dash. Applying nanotechnology to human health: Revolution in biomedical sciences. *Journal of Nanotechnology*, 2009, 2009: 1–14. https://doi.org/10.1155/2009/184702

[42] S. Khodadadi, N. Mahdinezhad, B. Fazeli-Nasab, et al. Investigating the possibility of green synthesis of silver nanoparticles using vaccinium arctostaphlyos extract and evaluating its antibacterial properties. *BioMed Research International*, 2021, 2021: 1−13. https://doi.org/10.1155/2021/5572252

[43] B. Mousavi, F. Tafvizi, Z.S. Bostanabad. Green synthesis of silver nanoparticles using *Artemisia turcomanica* leaf extract and the study of anti-cancer effect and apoptosis induction on gastric cancer cell line (AGS). *Artificial Cells*, *Nanomedicine*, *and Biotechnology*, 2018, 46(sup1):

499−510. https://doi.org/10.1080/21691401.2018.1430697
[44] S. Naghmouchi, M.I. Al-zaban, M. Al-zaben, et al. Generation and characterization of silver nanoparticles in mentha pulegium extract and evaluation of biological activities of the prepared extract. *Journal of Nanomaterials*, 2022, 2022: 1−8. https://doi.org/10.1155/2022/5410274
[45] L.B. Anigol, J.S. Charantimath, P.M. Gurubasavaraj. Effect of concentration and pH on the size of silver nanoparticles synthesized by green chemistry. *Organic and Medicinal Chemistry International Journal*, 2017, 3 (5): OMCIJ.MS.ID.555622.
[46] M. Amin, F. Anwar, M.R.S.A. Janjua, et al. Green synthesis of silver nanoparticles through reduction with solanum xanthocarpum L. berry extract: Characterization, antimicrobial and urease inhibitory activities against helicobacter pylori. *International Journal of Molecular Sciences*, 2012, 13(8): 9923−9941. https://doi.org/10.3390/ijms13089923
[47] A.M. Awwad, N.M. Salem. Green synthesis of silver nanoparticles byMulberry LeavesExtract. *Nanoscience and Nanotechnology*, 2012, 2(4): 125−128. https://doi.org/10.5923/j.nn.20120204.06
[48] N. Ahmad, Fozia, M. Jabeen, et al. Green fabrication of silver nanoparticles using euphorbia serpens kunth aqueous extract, their characterization, and investigation of its *in vitro* antioxidative, antimicrobial, insecticidal, and cytotoxic activities. *BioMed Research International*, 2022, 2022: 5562849. https://doi.org/10.1155/2022/5562849
[49] J. Balavijayalakshmi, V. Ramalakshmi. Carica papaya peel mediated synthesis of silver nanoparticles and its antibacterial activity against human pathogens. *Journal of Applied Research and Technology*, 2017, 15(5): 413−422. https://doi.org/10.1016/j.jart.2017.03.010
[50] H. Kaya, F. Aydin, M. Gürkan, et al. A comparative toxicity study between small and large size zinc oxide nanoparticles in tilapia (*Oreochromis niloticus*): Organ pathologies, osmoregulatory responses and immunological parameters. *Chemosphere*, 2016, 144: 571−582. https://doi.org/10.1016/j.chemosphere.2015.09.024
[51] P. Bélteky, A. Rónavári, N. Igaz, et al. Silver nanoparticles: Aggregation behavior in biorelevant conditions and its impact on biological activity. *International Journal of Nanomedicine*, 2019, 14: 667−687. https://doi.org/10.2147/IJN.S185965
[52] R. La Spina, D. Mehn, F. Fumagalli, et al. Synthesis of citrate-stabilized silver nanoparticles modified by thermal and pH preconditioned tannic acid. *Nanomaterials*, 2020, 10(10): 2031. https://doi.org/10.3390/nano10102031
[53] S. Jabariyan, M.A. Zanjanchi. Colorimetric detection of cadmium ions using modified silver nanoparticles. *Applied Physics A*, 2019, 125(12): 1−10. https://doi.org/10.1007/s00339-019-3167-7
[54] I.K. Siakavella, F. Lamari, D. Papoulis, et al. Effect of plant extracts on the characteristics of silver nanoparticles for topical application. *Pharmaceutics*, 2020, 12(12): 1244. https://doi.org/10.3390/pharmaceutics12121244
[55] N.V. Reddy, B.M. Satyanarayana, S. Sivasankar, et al. Eco-friendly synthesis of silver nanoparticles using leaf extract of Flemingia wightiana: Spectral characterization, antioxidant and anticancer activity studies. *SN Applied Sciences*, 2020, 2(5): 884. https://doi.org/10.1007/s42452-020-2702-7
[56] L. Sherin, A. Sohail, U. Amjad, et al. Facile green synthesis of silver nanoparticles using *Terminalia bellerica* kernel extract for catalytic reduction of anthropogenic water pollutants. *Colloid and Interface Science Communications*, 2020, 37: 100276. https://doi.org/10.1016/j.colcom.2020.100276
[57] D. Das, R. Ghosh, P. Mandal. Biogenic synthesis of silver nanoparticles using S1 genotype of Morus alba leaf extract: Characterization, antimicrobial and antioxidant potential assessment. *SN Applied Sciences*, 2019, 1(5): 1−16. https://doi.org/10.1007/s42452-019-0527-z
[58] R. Singh, C. Hano, G. Nath, et al. Green biosynthesis of silver nanoparticles using leaf extract of carissa carandas L. and their antioxidant and antimicrobial activity against human pathogenic bacteria. *Biomolecules*, 2021, 11(2): 299. https://doi.org/10.3390/biom11020299
[59] L.V. Hublikar, S.V. Ganachari, N. aghavendra, et al. Biogenesis of silver nanoparticles and its multifunctional anti-corrosion and anticancer studies. *Coatings*, 2021, 11(10): 1215. https://doi.org/10.3390/coatings11101215
[60] C. Gangwar, B. Yaseen, I. Kumar, et al. Growth kinetic study of tannic acid mediated monodispersed silver nanoparticles synthesized by chemical reduction method and its characterization. *ACS Omega*, 2021, 6(34): 22344−22356. https://doi.org/10.1021/acsomega.1c03100
[61] T. Begildayeva, S.J. Lee, Y. Yu, et al. Production of copper nanoparticles exhibiting various morphologies via pulsed laser ablation in different solvents and their catalytic activity for reduction of toxic nitroaromatic compounds. *Journal of Hazardous Materials*, 2021, 409: 124412. https://doi.org/10.1016/j.jhazmat.2020.124412
[62] M. Govindarajan, G. Benelli. One-pot green synthesis of silver nanocrystals using *Hymenodictyon orixense*: A cheap and effective tool against malaria, chikungunya and Japanese encephalitis mosquito vectors. *RSC Advances*, 2016, 6(64): 59021−59029. https://doi.org/10.1039/c6ra10228j
[63] L.A. Pham-Huy, H. He, C. Pham-Huy. Free radicals, antioxidants in disease and health. *International Journal of Biomedical Science*, 2008, 4(2): 89−96.
[64] P. Jadczak, D. Kulpa, R. Drozd, et al. Effect of AuNPs and AgNPs on the antioxidant system and antioxidant activity of lavender (lavandula angustifolia mill.) from *in vitro* cultures. *Molecules*, 2020, 25(23): 5511. https://doi.org/10.3390/molecules25235511
[65] M.M. Rahman, M.B. Islam, M. Biswas, et al. *In vitro* antioxidant and free radical scavenging activity of different parts of Tabebuia pallida growing in Bangladesh. *BMC Research Notes*, 2015, 8(1): 1–9. https://doi.org/10.1186/s13104-015-1618-6
[66] S. Yarrappagaari, R. Gutha, L. Narayanaswamy, et al. Eco-friendly synthesis of silver nanoparticles from the whole plant of Cleome viscosa and evaluation of their characterization, antibacterial, antioxidant and antidiabetic properties. *Saudi Journal of Biological Sciences*, 2020, 27(12): 3601−3614. https://doi.org/10.1016/j.sjbs.2020.07.034
[67] N.B. Gaber, S.I. El-Dahy, E.A. Shalaby. Comparison of ABTS, DPPH, permanganate, and methylene blue assays for determining antioxidant potential of successive extracts from pomegranate and guava residues. *Biomass Conversion and Biorefinery*, 2023, 13(5): 4011−4020. https://doi.org/10.1007/s13399-021-01386-0
[68] R.M. Mangoale, A.J. Afolayan. Comparative phytochemical constituents and antioxidant activity of wild and cultivated *Alepidea amatymbica* eckl & zeyh. *BioMed Research International*, 2020, 2020: 5808624. https://doi.org/10.1155/2020/5808624
[69] D. Randriamampionona, B. Diallo, F. Rakotoniriana, et al. Comparative analysis of active constituents in *Centella asiatica* samples from Madagascar: Application for *ex situ* conservation and clonal propagation. *Fitoterapia*, 2007, 78(7/8): 482–489. https://doi.org/10.1016/j.fitote.2007.03.016
[70] R. Mata, J.R. Nakkala, S.R. Sadras. Biogenic silver

nanoparticles from *Abutilon indicum*: Their antioxidant, antibacterial and cytotoxic effects *in vitro*. *Colloids and Surfaces B*: *Biointerfaces*, 2015, 128: 276–286. https://doi.org/10.1016/j.colsurfb.2015.01.052

[71] B. Kumar, K. Smita, L. Cumbal, et al. Phytosynthesis and photocatalytic activity of magnetite (Fe_3O_4) nanoparticles using the Andean blackberry leaf. *Materials Chemistry and Physics*, 2016, 179: 310−315. https://doi.org/10.1016/j.matchemphys.2016.05.045

[72] F. Samari, H. Salehipoor, E. Eftekhar, et al. Low-temperature biosynthesis of silver nanoparticles using mango leaf extract: Catalytic effect, antioxidant properties, anticancer activity and application for colorimetric sensing. *New Journal of Chemistry*, 2018, 42(19): 15905−15916. https://doi.org/10.1039/C8NJ03156H

[73] N. Mohanapriya, S. Murugesan, V. Sivamurugan. *In vitro* α-amylase and α-glucosidase inhibitory activity of methanol extract of tolypiocladia glomerulata. *Saudi Journal of Biomedical Research*, 2016, 1(3): 59–63.

[74] M. Amin Mir, S. S. Sawhney, M. M. S Jassal. *In-vitro* antidiabetic studies of various extracts of Taraxacum officinale. *The Pharma Innovation*, 2015, 4(1): 61–66.

[75] S.M. Firdous. Phytochemicals for treatment of diabetes. *EXCLI Journal*, 2014, 13: 451−453. https://doi.org/10.17877/DE290R-15666

[76] L. Oprica, M. Andries, L. Sacarescu, et al. Citrate-silver nanoparticles and their impact on some environmental beneficial fungi. *Saudi Journal of Biological Sciences*, 2020, 27(12): 3365−3375. https://doi.org/10.1016/j.sjbs.2020.09.004

[77] A. Shah, M. Ahmed, N. Mushtaq, et al. Kinetic and inhibitory effect of Silene arenosa extracts against pancreatic α amylase. *International Journal of Botany Studies*, 2019, 4(4): 78−82.

[78] T.L. Rosenberry, J.L. Johnson, B. Cusack, et al. Interactions between the peripheral site and the acylation site in acetylcholinesterase. *Chemico-Biological Interactions*, 2005, 157/158: 181–189. https://doi.org/10.1016/j.cbi.2005.10.027

[79] M.B. Colović, D.Z. Krstić, T.D. Lazarević-Pašti, et al. Acetylcholinesterase inhibitors: Pharmacology and toxicology. *Current Neuropharmacology*, 2013, 11(3): 315−335. https://doi.org/10.2174/1570159x11311030006

[80] J. Panchal, M. Islam, K. DeBoeuf, et al. Signaling mechanisms underlying nicotine-induced upregulation of α7 nicotinic acetylcholine receptor (nAChR). *Biophysical Journal*, 2020, 118(3): 420a. https://doi.org/10.1016/j.bpj.2019.11.2371

[81] N. Sher, M. Ahmed, N. Mushtaq, et al. Enhancing antioxidant, antidiabetic, and antialzheimer performance of *Hippeastrum hybridum* (L.) using silver nanoparticles. *Applied Organometallic Chemistry*, 2022, 36(7): e6724. https://doi.org/10.1002/aoc.6724

[82] D. McShan, P.C. Ray, H.T. Yu. Molecular toxicity mechanism of nanosilver. *Journal of Food and Drug Analysis*, 2014, 22(1): 116−127. https://doi.org/10.1016/j.jfda.2014.01.010

[83] A. Khatoon, F. Khan, N. Ahmad, et al. Silver nanoparticles from leaf extract of *Mentha piperita*: Eco-friendly synthesis and effect on acetylcholinesterase activity. *Life Sciences*, 2018, 209: 430−434. https://doi.org/10.1016/j.lfs.2018.08.046

[84] A. Shah, M. Ahmed, N. Sher, et al. Efficacy of Silene arenosa extract on acetylcholinesterase in *Bungarus sindanus* (krait) venom. *Journal of Traditional Chinese Medicine*, 2021, 41(3): 349−354. https://doi.org/10.19852/j.cnki.jtcm.2021.03.001

© The author(s) 2023. This is an open-access article distributed under the terms of the Creative Commons Attribution 4.0 International License (CC BY) (http://creativecommons.org/licenses/by/4.0/), which permits unrestricted use, distribution, and reproduction in any medium, provided the original author and source are credited.